This article has been accepted for publication in a future issue of this journal, but has not been fully edited. Content may change prior to final publication. Citation information: DOI10.1109/PAINE56030.2022.10014840, 2022 IEEE Physical Assurance and Inspection of Electronics (PAINE)

Printed circuit board inspection: Fusion of optical and X-ray images (FOXi) for electronic components classification

Dmitrii Starodubov
College of Engineering, Design and Physical Sciences, Brunel University
London, U.K.
dmitry_starodubov@hotmail.com

Sebelan Danishvar
College of Engineering, Design and Physical Sciences, Brunel University
London, U.K.
sebelan.danishvar@brunel.ac.uk

Richard Ott
Air Force Research Laboratory, Sensors Directorate
WPAFB, OH, USA.
richard.ott.3@us.af.mil

Abd Al Rahman M. Abu Ebayyeh
Department of Electrical and Electronic Engineering, Imperial College, London, U.K.
a.abu-ebayyeh@imperial.ac.uk

Noel Cummings
Scanna MSC Ltd
London, U.K.
noelc@scanna-msc.com

Alireza Mousavi
College of *Engineering, Design and Physical Sciences, Brunel University*
London, U.K.
alireza.mousavi@brunel.ac.uk

***Abstract*— The effective and efficient quality, security and provenance assurance of microelectronics and electronic products is a persisting challenge for the industry. The impetus towards finding automatic solutions that create high confidence about the quality and origin of components assembled on Printed Circuit Boards (PCBs) is high. A novel approach is proposed for microelectronic component detection and classification with high accuracy and confidence. A dedicated multi-source data acquisition, fusion and interpretation, are suggested to reduce uncertainty regarding concurrency, reliability, availability, and physical/logical resolution. Increasing the quality of data and subsequently generating the infrastructure for knowledge creation is the main output of this research. A central feature of the proposed solution is the integration and fusion of images from surface and penetrating imaging systems, set specifically to generate the necessary raw data. Experiments reported here demonstrate the merits of the accomplished classification, learning and identification of constituent components through the proposed fusion algorithm[1]. The accuracy of the analytics from the fusion of optical and X-ray algorithms has improved by 5.3%, compared to optics only. All other sensitivities were also significantly improved; for example, the Chip sensitivity in optical and X-ray images was 89.4% and 85.8%, respectively. With FOXi the metric increased to 94%.**

Keywords—Bill of materials (BoM), Image fusion, Classification, Convolutional neural network (CNN), PCB boards, Components.

I. INTRODUCTION

A bill of materials (BoM) is the comprehensive list of raw materials, components, and instructions necessary for the manufacture, repair, or construction of a product. Typically, BOMs are structured in a hierarchical format so that the completed product appears on top and the individual materials and components follow [1, 2].

BoM of a PCB (Printed Circuit Board) can be a list of components such as resistors, capacitors, Integrated Circuits (I.C.s), ports, connectors etc. BoMs are used for a wide range of applications, including electronic board inspection and quality assurance, security and technical auditing.

Previous research has described various automatic PCB inspection methods that use optical/visual cameras, X-ray sources, thermal cameras, etc. The authors have also witnessed industrial solutions that have not been publicly reported but show effective industrial capabilities. A variety of image processing, computer vision, and machine learning techniques are employed in these studies and industrial applications. Many existing methods focus on defect inspection and detection, solder inspection, pose detection, quality inspection and PCB classification [3-7]. From our studies and reviews of publicly accessible articles, it appears that the approach to solving the problem is restricted to the monomodal imaging technique for obtaining data from the boards, and no significant work is done to classify the electronic components on the boards.

This paper aims to find novel approaches for ensuring the minimum information necessary to control and minimize uncertainty during the registration and fusion of data in contrast with a systematic methodological inquiry to improve the performance of component classification.

We, therefore, suggest the utilization and management of multiple data sources to reduce uncertainty in terms of concurrency, reliability, availability, and physical/logical resolution. Our research focuses on building a foundation framework for quality assurance and developing a systematic knowledge infrastructure. This is a computational framework that evaluates the efficacy, value, and application of observable-available information into the state of a given physical system.

There are several potential threats to sensitive systems, including tampering, hidden components, and broken provenance. As part of this study, we examine the suitability of data acquisition (X-ray and optical surface imaging

[1] Patent: Entropic Greyscale Imaging (Object Identification System and Method)/JE/N36998-GB

This article has been accepted for publication in a future issue of this journal, but has not been fully edited. Content may change prior to final publication. Citation information: DOI10.1109/PAINE56030.2022.10014840, 2022 IEEE Physical Assurance and Inspection of Electronics (PAINE)

technologies) and image processing to further improve the capability for detecting components and systems in electronic systems. In the following sections, we describe the proposed methodology.

II. Proposed Approach

A. Image acquisition

An optical camera and X-ray imaging system are used to acquire the necessary images/data in this study. One hundred circuit boards in this study span a range of sizes from $70mm \times 50mm$ to $350mm \times 250mm$ (e.g., Fig. 1).

A high-resolution professional camera is used for the surface acquisition system, which is equipped with two lenses with focal lengths of 35 mm and 12 mm. The resolution of all images is $5496\ (H) \times 3672\ (V)$ pixels. A physical barrier controls outside light so that the optical system can provide constant illumination.

X-ray machines are the most effective method for inspecting inside electronic components due to their penetrating abilities. A specialized and tweaked X-ray scanner is used to provide the images with a resolution of $3840\ (H) \times 3072\ (V)$ pixels.

The images from multiple sensors need to be registered to achieve multi-sensor fusion. A useful feature that helps distinguish devices from backgrounds is device boundaries, which are used in this research to match images between optical and X-rays. This paper assumes that the images to be fused are correctly registered.

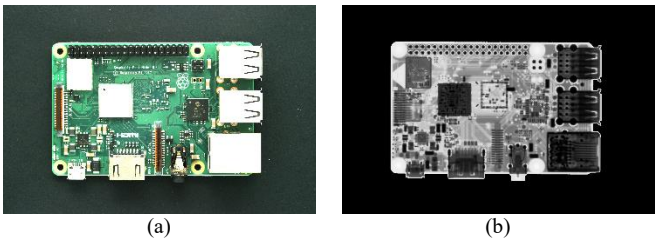

(a) (b)

Fig. 1. An example of an optical image (a) and X-ray image (b) which are taken from a Raspberry Pi board.

B. Image preparation

In order to train the neural network and to classify components in this research, we require components images of 128×128 pixels. These images are acquired by resizing the source image (Optical, X-ray and fused images) regions where components are located. Thus, optical images of devices are labelled accordingly. The labelling process is time-consuming if performed by humans. Therefore, we suggested and developed a component image extraction algorithm based on common image processing functions and special hue analysis.

1. Pre-processing

To remove noise and reduce image sharpness median blur function is applied to optical images. The kernel for the function is square with a side of 25 pixels for an image size of 5496×3672 pixels.

2. Colour space conversion

Due to the conditions of capturing images, the background's hue is always different to the hue/hues of most of the device area. Although, in most cases, the hues of components differ from those of a circuit board surface, they are sometimes similar. In case of similarity, another method for component detection is used where intensity is analyzed. Detection on the optical image is not feasible (even by humans) if some components have the same colour as the circuit board surface.

To improve the detection of hues in both background and target objects, RGB colour space is converted into a custom colour space. This conversion allows mitigating shadows and other intensity changes (or red, green, and blue components) across the background. New components are shown using Algorithm (1).

These equations consider R, G, and B values in a range of $0 \ldots 255$. If the range is $0 \ldots 1$, 0.5 should be used instead of 127 and 128 [8].

```
I = (R + G + B) / 3 // similar to intensity or brightness
RI = if (I = 0) then 127 else 127 + max(-127, min(128, ln(R / I) * 127))
GI = if (I = 0) then 127 else 127 + max(-127, min(128, ln(G / I) * 127))
BI = if (I = 0) then 127 else 127 + max(-127, min(128, ln(B / I) * 127))
```

Algorithm (1)

3. Distributions for background/circuit board surface colour and max detection

At this stage, I, RI, G.I., and B.I. distributions for background or circuit board are calculated. Since the device is located in the centre of the image, it is possible to use an area in the form of a wide frame along the borders of the image to calculate the distribution of I, RI, G.I., and B.I. for background. We used a frame with 100 pixels in width. Component locations are unknown, and almost the whole device area is used to calculate distributions for circuit board surface colour. Components are considered to have a smaller surface area than circuit boards.

The result of the calculation is four arrays of length 256. These arrays are used to detect thresholds for background or circuit board surface segmentation. A median filter with a kernel of 13 is applied to each distribution. This filter helps to suppress maximums related to sets of one-coloured components and emphasizes the maximum of the target area. This maximum could be stretched in raw distribution due to shadows and lighting conditions. Then, maximums are calculated for each distribution: MI, MRI, MGI, and MBI [9].

4. Threshold segmentation

For each pixel of the image area of interest, a decision is made whether the pixel belongs to the target area (background or circuit board surface) or not (device or component). The decision is based on thresholds (minTI, maxTI, minTRI, maxTRI, minTGI, maxTGI, minTBI, maxTBI) and other comparisons based on pixel I, RI, G.I.,

This article has been accepted for publication in a future issue of this journal, but has not been fully edited. Content may change prior to final publication. Citation information: DOI10.1109/PAINE56030.2022.10014840, 2022 IEEE Physical Assurance and Inspection of Electronics (PAINE)

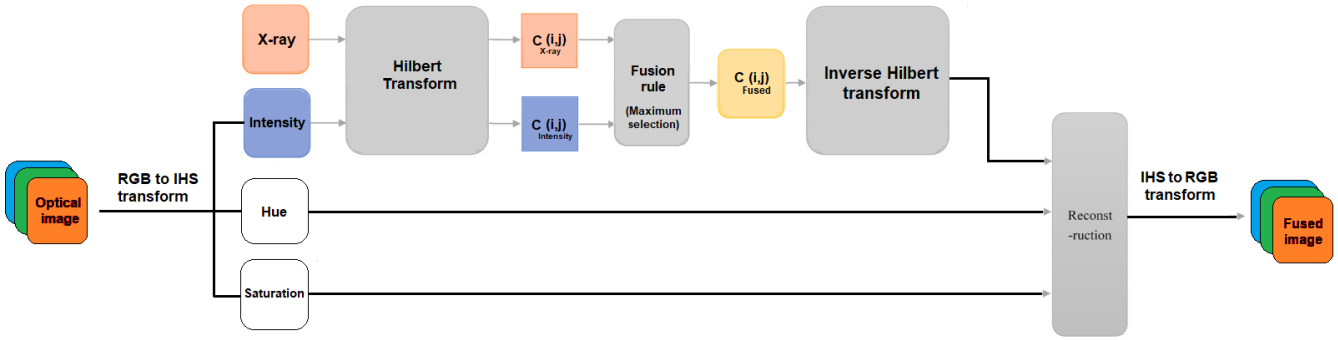

Fig. 2. Block diagram of Hilbert-IHS fusion method

B.I. values, and maximums of distributions acquired in the previous step. The threshold condition is "if pixel I, RI, G.I., B.I. are within ranges minTN... maxTN, the pixel belongs to background or circuit board surface". The threshold condition is used in conjunction or disjunction with other custom conditions.

4.1 Threshold segmentation for revealing background and device mask

For background, the thresholds are evaluated using Algorithm (2). All fixed parameters in these algorithms are achieved based on dataset conditions and experiments.

```
minD = 16
maxD = 64
minDR = if MRI < 127 then min(maxD, minD + 127 - MRI) else minD
minDG = if MGI < 127 then min(maxD, minD + 127 - MGI) else minD
minDB = if MBI < 127 then min(maxD, minD + 127 - MBI) else minD
maxDR = if MRI > 127 then min(maxD, minD - 127 + MRI) else minD
maxDG = if MGI > 127 then min (maxD, minD - 127 + MGI) else minD
maxDB = if MBI > 127 then min (maxD, minD - 127 + MBI) else minD
minTI = 0
maxTI = MI + 32
minTRI = MRI - minDR
maxTRI = MRI + maxDR
minTGI = MGI - minDG
maxTGI = MGI + maxDG
minTBI = MBI - minDB
maxTBI = MBI + maxDB
```

Algorithm (2)

These deltas (minDR, maxDR etc.) extend value ranges in a direction equal to the difference between 127 and distribution maximums.
If the background pixel does not pass the thresholds, Algorithm (3) is applied.

```
MRG = MRI - MGI
MGB = MGI - MBI
MRB = MRI - MBI
if (MRG > 16 and MRB > 16) // red background
   if (MGB >= 0) // green is between blue and red for background
      if (RI - GI >= MRG / 2 and GI - BI >= MGB / 2)
         pixel is background
   else // blue is between green and red for background
      if (RI - BI >= MRB / 2 and BI - GI >= -MGB / 2)
         pixel is background
if (-MRG > 16 and MGB > 16) // green background
   if (MRB >= 0) // red is between blue and green for background
      if (GI - RI >= -MRG / 2 and RI - BI >= MRB / 2)
         pixel is background
   else // blue is between red and green for background
      if (GI - BI >= MGB / 2 and BI - RI >= -MRB / 2)
         pixel is background
if (-MGB > 16 and -MRB > 16) // blue background
   if (-MRG >= 0) // green is between red and blue for background
      if (BI - GI >= -MGB / 2 and GI - RI >= -MRG / 2)
         pixel is background
   else // red is between green and blue for background
      if (BI - RI >= -MRB / 2 and RI - GI >= MRG / 2)
         pixel is background
```

Algorithm (3)

The idea of applying these conditions is that if differences between pixel components are similar to differences between distribution maximums, the pixel belongs to the background.

4.2 Threshold segmentation for revealing circuit board surface

For background, the thresholds are evaluated using the following equations:

```
minTI = 0                                                    (1)
maxTI = 192
minTRI = MRI - 48
maxTRI = MRI + 48
minTGI = MGI - 48
maxTGI = MGI + 48
minTBI = MBI - 48
maxTBI = MBI + 48
```

If the pixel passes the thresholds for the circuit board surface, the conditions in Algorithm (4) are applied.

```
HRG = MRI - MGI > 32 // red >> green
HRB = MRI - MBI > 32 // red >> blue
HGR = MGI - MRI > 32 // green >> red
HGB = MGI - MBI > 32 // green >> blue
HBG = MBI - MGI > 32 // blue >> green
HBR = MBI - MRI > 32 // blue >> red
if ((RI < GI and HRG) and (RI < BI v HRB) and (GI < RI and HGR > 32) and (GI < BI and HGB > 32) and (BI < GI and HBG > 32) and (BI < RI and HBR > 32))
   pixel is not circuit board surface
```

Algorithm (4)

This article has been accepted for publication in a future issue of this journal, but has not been fully edited. Content may change prior to final publication. Citation information: DOI10.1109/PAINE56030.2022.10014840, 2022 IEEE Physical Assurance and Inspection of Electronics (PAINE)

The idea of applying this condition is that if differences between pixel components are opposite to considerable differences between distribution maximums, the pixel does not belong to the circuit board surface.

5. Background threshold segmentation post-processing

The post-processing depends on the colour of the background. If (|MRI - 127| + |MGI - 127| + |MBI - 127|) > 48 background colour saturation is high, and it is low otherwise. If the saturation is high, the biggest connected component on the binary mask is considered as a device, and then a morphological operation is executed to remove noise [10]. If the saturation is low, all small holes are removed on the connected component before filtering the biggest connected component (these holes are usually greyscale components of a device), and closing is not executed.

6. Customization of threshold segmentation for revealing circuit board surface

A specified area of the device binary mask (area of interest) is segmented, not the entire image. The following regions of the mask are excluded from the calculation of distributions: high intensity (white components, light reflection) regions and low saturation regions (excluding random false maximums).

7. Circuit board surface segmentation post-processing

By subtracting the circuit board surface binary mask from the device binary mask, the component binary mask is obtained. However, close components are usually connected, and the mask contains many minor artefacts. To separate components, morphological opening and closing are executed. To remove artefacts, all small particles and holes with a size of fewer than 400 pixels are removed. Then, morphological erosion is applied again to separate the remaining connected components on the mask. This post-processing fails to separate components if there is no space (circuit board surface) between the components on the image. To fix this problem, gradient and texture analysis is required for more precise post-processing.

The final stage is a component binary mask. This mask is used to extract component images from source optical or X-ray images and classify the component.

C. Image Fusion

Fusion is the process of merging two or more images into one. In image fusion, all relevant, significant, and related information is preserved from each input image.

In general, multi-modal image fusion involves combining information from various input sources taken from specific objects into a single image; the result is known as the fused image. Fused images provide breadth and depth data [11].

Optical (RGB image) and X-ray (Monochrome) images extracted from boards are fused using two-dimensional Hilbert transform (2-D H.T.) and intensity-hue-saturation (IHS). By applying the Hilbert transform, we can derive the minimum-phase response from a spectral analysis. The Hilbert transform of *f(t)* is the convolution of *f(t)* with the function $h(t) = \frac{1}{\pi t}$. Therefore, the Hilbert transform of a signal *f(t)* is given by:

$$H(f)(t) = \frac{-1}{\pi} \lim_{\varepsilon \to 0} \int_{\varepsilon}^{\infty} \frac{f(t+\tau) - f(t-\tau)}{\tau} d\tau \qquad (2)$$

The Hilbert Transform is widely used in one-dimensional versions for various applications; in the case of 2D images, several approaches have been developed. The method presented in this paper takes its inspiration from [12].

There are six steps in the image fusion process:

Step 1. Converting the colour optical image from RGB space to IHS space.

Step 2. Separating the intensity component (I) of optical image in the IHS domain (The hue (H) and saturation (S) remain unchanged during the fusion process.)

Step 3. Applying two-dimensional Hilbert transform (2-D H.T.) to the X-ray and the intensity component (I) of optical images.

Step 4. Employing the maximum fusion rules to combine the two-dimensional Hilbert transform (2-D H.T.) coefficients of input images.

Step 5. Achieving the new intensity component by applying the inverse Hilbert transform.

Step 6. Illustrating the fused image in RGB space utilizing an IHS to RGB algorithm.

Fig. 2 illustrates the fusion process in block diagram form. The results of the integration of two images are shown in Fig. 3. Fig. 4 depicts a zoomed version of a chip on the input images and the resulting image.

Fig. 3. Fused image archived by integration of images shown in Fig. 1.

(a)

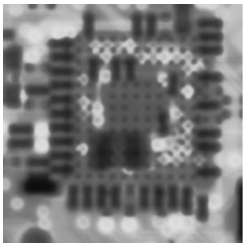

(b)

This article has been accepted for publication in a future issue of this journal, but has not been fully edited. Content may change prior to final publication. Citation information: DOI10.1109/PAINE56030.2022.10014840, 2022 IEEE Physical Assurance and Inspection of Electronics (PAINE)

(c)

Fig. 4. A chip image cropped from the board, optical image (a), X-ray image (b), and fused image (c).

D. *Convolutional Neural Networks (CNN) classifier*

CNNs are a type of deep neural network commonly used in computer vision and image classification. The CNN uses multiple building blocks, such as convolutional layers, pools of features, and fully connected layers, to automatically learn the spatial hierarchy of features through backpropagation.

There are three layers in CNNs: an input layer, an output layer, and a hidden layer. In general, hidden layers are made up of convolutional, ReLU, pooling, fully connected layers, and activation layer functions [13, 14].

- Input is convolutionally processed by convolutional layers. Information is passed from this layer to the next.
- In the next layer, pooling is used to combine the outputs of multiple neurons into a single neuron.
- Every neuron in one layer is connected to every neuron in the next layer, forming fully connected layers.

CNNs extract features from images. As a result, manual feature extraction is no longer necessary, and while the network is training on images, these are learned. Therefore, for computer vision tasks, deep learning models are highly reliable. With tens or hundreds of hidden layers, CNNs are trained to detect features. Learning features become more complex with each layer.

Fig. 5 demonstrates the CNN architecture used in this paper. Input images size is 128 × 128 pixels, and kernel size is 3. The number of output classes is five.

A summary of the 2D-CNN with two convolutional layers and three fully connected layers is shown in Fig. 6.

III. Results

In this section, we evaluate the performance of the CNN classifier to classify components in three groups of data: optical images, X-ray images and fused images.

In each group of data, there are five balanced classes: chips, connectors, others, ports, and two-solders. Each component image in the dataset has a dimension of 128 by 128 pixels. The total data used for each group is 24,000 components which are divided into 20,000 training data, 4,000 validation data, and 4,000 test data. Using these data groups

Model: "sequential"

Layer (type)	Output Shape	Param #
conv2d (Conv2D)	(None, 126, 126, 64)	1792
max_pooling2d (MaxPooling2D)	(None, 63, 63, 64)	0
conv2d_1 (Conv2D)	(None, 61, 61, 128)	73856
max_pooling2d_1 (MaxPooling 2D)	(None, 30, 30, 128)	0
flatten (Flatten)	(None, 115200)	0
dropout (Dropout)	(None, 115200)	0
dense_1 (Dense)	(None, 128)	14745728
dense_2 (Dense)	(None, 32)	4128
dense_3 (Dense)	(None, 5)	165

Total params: 14,825,669
Trainable params: 14,825,669
Non-trainable params: 0

Fig. 6. Summary of the 2D-CNN and parameters

allow us to explore the influence of image fusion on CNN classifier and classification performance.

Throughout this study, accuracy, recall (Sensitivity),

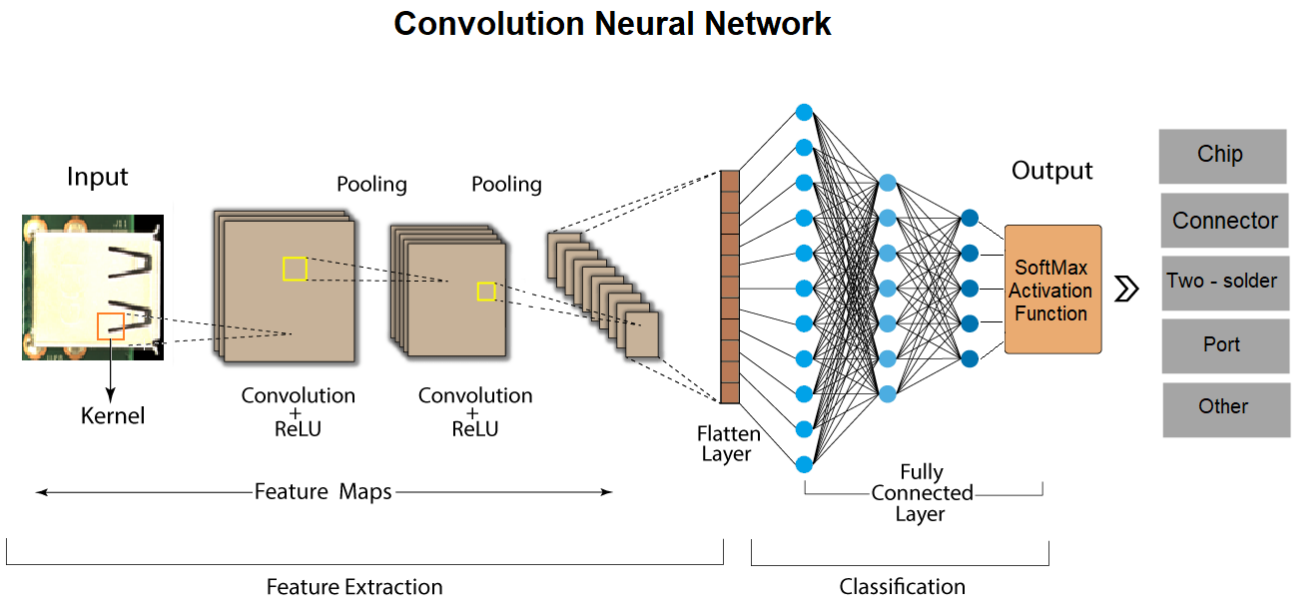

Fig. 5. Proposed CNN architecture

This article has been accepted for publication in a future issue of this journal, but has not been fully edited. Content may change prior to final publication. Citation information: DOI10.1109/PAINE56030.2022.10014840, 2022 IEEE Physical Assurance and Inspection of Electronics (PAINE)

precision, and F1-score metrics are employed to evaluate the performance of these methods. The accuracy calculates how many images will be correctly classified. Using the precision, we can estimate the exact efficiency of our Algorithm for predicting positive samples. True positives are measured by the recall, and the F1 score calculates the mean harmonic of recall and precision. Using the confusion matrix, it is possible to calculate the four performance measurements: true positive (T.P.), true negative (T.N.), false negative (F.N.) and false positive (F.P.).

On the basis of equations (2) to (5), accuracy, precision, recall, and F1 score are determined.

$$Accuracy = \frac{TN+TP}{TN+FN+TP+FP} \quad (2)$$

$$Sensitivity = \frac{TP}{TP+FN} \quad (3)$$

$$Precision = \frac{TP}{TP+FP} \quad (4)$$

$$F1-score = \frac{2\times(Precision\times Sensitivity)}{Precision+Sensitivity} \quad (5)$$

Tables I to III show the test data performances result for all three groups.

Based on these results, the proposed approach and fusion of optical and X-ray data improve classifier results. It can be observed that the fusion strategy has the best accuracy (91%), which improves optical data accuracy by 5.3%. Comparing the other metrics in the tables, we find that these improvements are observed in all individual classes as well. For example, Chips' sensitivity in optical and X-ray images is 89.4% and 85.8%, respectively. As a result of combining the data, this metric increases to 94%.

It can be reasonably assumed that surface and colour information from optical images combined with penetrating information from X-ray images has contributed to these results.

TABLE I. ACCURACY, SENSITIVITY, PRECISION, AND F1-SCORE METRICS FOR OPTICAL DATA

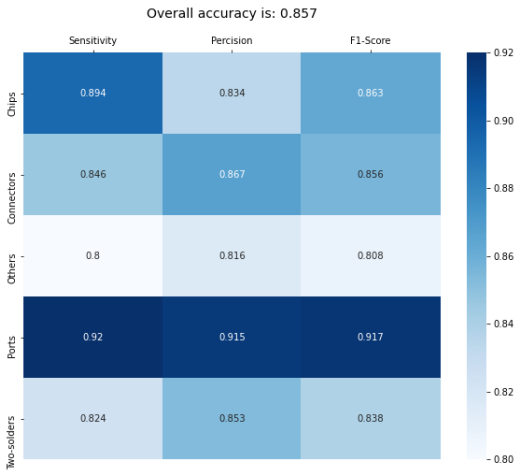

TABLE II: ACCURACY, SENSITIVITY, PRECISION, AND F1-SCORE METRICS FOR X-RAY DATA

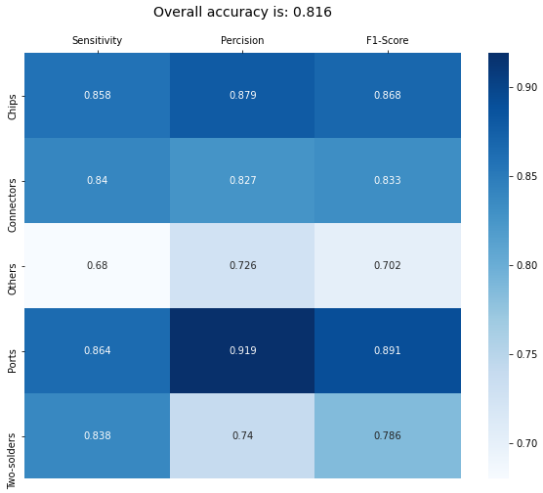

TABLE III: ACCURACY, SENSITIVITY, PRECISION, AND F1-SCORE METRICS FOR FUSED DATA

ACKNOWLEDGEMENTS

The research programme is sponsored and supported by the United States Air Force Office of Scientific Research (AFOSR), Air Force Research Lab (AFRL) and Sensors Directorate (SY).

REFERENCES

[1] A. A. R. M. A. Ebayyeh and A. Mousavi, "A Review and Analysis of Automatic Optical Inspection and Quality Monitoring Methods in Electronics Industry," in IEEE Access, vol. 8, pp. 183192-183271, 2020, doi: 10.1109/ACCESS.2020.3029127.

[2] N. T. Jessurun, O. P. Dizon-Paradis, M. Tehranipoor and N. Asadizanjani, "SHADE: Automated Refinement of PCB Component Estimates Using Detected Shadows," 2020 IEEE Physical Assurance and Inspection of Electronics (PAINE), 2020, pp. 1-6, doi: 10.1109/PAINE49178.2020.9337564.

[3] J. Li, W. Li, Y. Chen and J. Gu, "A PCB Electronic Components Detection Network Design Based on Effective Receptive Field Size and Anchor Size Matching", Computational Intelligence and Neuroscience, vol. 2021, 19 pages, 2021, doi: 10.1155/2021/6682710.

[4] L. Haochen, Z. Bin, S. Xiaoyong and Z. Yongting, "CNN-Based Model for Pose Detection of Industrial PCB," 2017 10th International Conference on Intelligent Computation Technology and Automation (ICICTA), 2017, pp. 390-393, doi: 10.1109/ICICTA.2017.93.

[5] V. Mankad, N. Bhanvadia, M. I. Patel and R. Gajjar, "PCB Classification using Convolutional Neural Network," 2021 3rd International Conference on Advances in Computing, Communication Control and Networking (ICAC3N), 2021, pp. 986-990, doi: 10.1109/ICAC3N53548.2021.9725695.

[6] C. Bo, H. Hu, J. Xu, Z. Liu and P. Chai, "Classification learning method for PCB insertion holes based on shape context," 2017 3rd IEEE International Conference on Computer and Communications (ICCC), 2017, pp. 1933-1937, doi: 10.1109/CompComm.2017.8322875.

[7] G. Ran, X. Lei, D. Li and Z. Guo, "Research on PCB Defect Detection Using Deep Convolutional Neural Network," 2020 5th International Conference on Mechanical, Control and Computer Engineering (ICMCCE), 2020, pp. 1310-1314, doi: 10.1109/ICMCCE51767.2020.00287.

[8] K. Inoue, M. Jiang and K. Hara, "Hue-Preserving Saturation Improvement in RGB Color Cube" Journal of Imaging. 2021 Aug 18;7(8):150. Doi: 10.3390/jimaging7080150.

[9] B. Wang and C. L. P. Chen, "An Effective Background Estimation Method for Shadows Removal of Document Images," 2019 IEEE International Conference on Image Processing (ICIP), 2019, pp. 3611-3615, doi: 10.1109/ICIP.2019.8803486.

[10] N. Jamil, T. M. T. Sembok and Z. A. Bakar, "Noise removal and enhancement of binary images using morphological operations," 2008 International Symposium on Information Technology, 2008, pp. 1-6, doi: 10.1109/ITSIM.2008.4631954.

[11] S. Daneshvar and H. Ghassemian, "MRI and PET image fusion by combining IHS and retina-inspired models," Information Fusion, Elsevier, Vol. 11, No. 2, pp. 114-123, 2010, doi: 10.1016/j.inffus.2009.05.003

[12] M. Haddadpour, S. Daneshvar and H. Seyedarabi, "PET and MRI image fusion based on combination of 2-D Hilbert transform and IHS method, Biomedical Journal," Vol 40, No. 4, 2017,doi: 10.1016/j.bj.2017.05.002.

[13] Y. Zhang, L. Yuan, K. Yang and P. Liu, "Hyperspectral Image Classification Based on CNN with Spectral-Spatial features," 2021 International Conference on Computer Information Science and Artificial Intelligence (CISAI), 2021, pp. 956-959, doi: 10.1109/CISAI54367.2021.00192

[14] A. A. R. M. Abu Ebayyeh, S. Danishvar and A. Mousavi, "An Improved Capsule Network (WaferCaps) for Wafer Bin Map Classification Based on DCGAN Data Upsampling," in IEEE Transactions on Semiconductor Manufacturing, vol. 35, no. 1, pp. 50-59, Feb. 2022, doi: 10.1109/TSM.2021.3134625.